Heliyon 9 (2023) e17429

Contents lists available at ScienceDirect

Heliyon

journal homepage: www.cell.com/heliyon

Tunable luminescence and electrical properties of cerium doped strontium aluminate ($SrAl_2O_4:Ce^{3+}$) phosphors for white LED applications

Ganesh Kumar K [a,*], Balaji Bhargav P [b], Sasikumar P [a], Anitha Gopalan [c], Pugazhendhi S [a], Mary Anjalin F [a], Vimalan M [a,**], Mohamed Abbas [d,***]

[a] Department of Physics, Saveetha School of Engineering, SIMATS, Thandalam, Chennai, 602105, India
[b] Department of Physics, Sri Sivasubramaniya Nadar College of Engineering, Kalavakkam, Tamilnadu, 603110, India
[c] Department of VLSI Microelectronics, Saveetha School of Engineering, SIMATS, Thandalam, Chennai, 602105, India
[d] Electrical Engineering Department, College of Engineering, King Khalid University, Abha, 61421, Saudi Arabia

ARTICLE INFO

Keywords:
Optical
Morphology
White phosphor
Photoluminescence
Dielectric

ABSTRACT

In new research growth long after glow material is a potential candidate due to its physical properties, chemical stability and wide application in modern solid-state lightning (LED), display devices, dosimetry and sensors. A cerium doped strontium aluminate phosphor ($SrAl_2O_4:Ce^{3+}$) was synthesized by conventional solid-state reaction method. The crystal structure and morphology of phosphors, while doping rare earth metal and lithium metal ion was investigated by using X-ray diffraction, Raman spectroscopy and field emission scanning electron microscopy. Fourier transformed infrared spectrum results of the synthesized phosphor composition conforms the characteristic vibration bands of synthesized phosphor. Surface composition analysis of the prepared samples was examined using X-ray photoelectron spectroscopy. Photoluminescence emission band observed at ~420 nm, ~490 nm and ~610 nm region under the excitation wavelength of 256 nm. Wight light emission was confirmed using the Commission Internationale de L'Eclairage (CIE) chromatic coordinate graph. The correlated colour temperature (CCT) value of 0.5% Ce^{3+} doped SAO of phosphors was calculated is in the range of 1543 K, which is indicated the synthesized phosphors performance as warm white light source. The obtained phosphor has a high dielectric constant and low loss tangent which is useful to optoelectronic devices.

1. Introduction

Rare-earth doped alkaline earth aluminates have sought high interest in the modern research community for their stable thermal and chemical properties, and long-after-glow phosphorescence. They can be widely used for lighting applications in the automobile and electronic industries [1]. Among the various rare earth aluminate phosphor material, $SrAl_2O_4$ (SAO) is considered to be the foremost promising base material when blended with rare earth metal ions [2] due to its increased brightness, safety, long duration,

* Corresponding author.
** Corresponding author.
*** Corresponding author.
E-mail addresses: aeroganesh.mcc@gmail.com (G. Kumar K), myresearch1121@gmail.com (V. M), mabas@kku.edu.sa (M. Abbas).

https://doi.org/10.1016/j.heliyon.2023.e17429
Received 8 May 2023; Received in revised form 15 June 2023; Accepted 16 June 2023
Available online 20 June 2023

and minimal toxicity [3]. Alkaline aluminate ($SrAl_2O_4$) associated with the tridymite structure, space group (P_{21}), and AlO_4 tetrahedral vibration [4] are synthesized on a large scale by solid-state reaction method for its reproducibility. Kim et al. reported different doping compositions of $SrAl_2O_4$:Eu^{2+}, Dy^{3+} green emitting phosphors [5,6]. Cerium (Ce^{3+}) doped aluminate phosphors are used in fast scintillators and long-after-glow (LAG) phosphorescent materials. From the 5d-4f transition, the emission of a broad spectrum with two peaks was observed under a long wavelength UV region [7]. Li et al. reported the emission spectrum of solid-state synthesized Ce^{3+} doped $Sr_3Al_2O_6$ phosphor with broad emission peaks centered at 455 nm and 487 nm [8]. Combustion synthesized Ce^{3+} doped $SrAl_2O_4$ white light emission phosphors, resulting in the simultaneous blue and green-yellow band emission at 0.5% of Ce^{3+}. The addition of the flux of H_3BO_3, the inhibitor of Ce, and the charger compensator of Li^+ results in the synthesis of a novel green phosphor of $SrAl_2O_4$: Eu^{2+}, Ce^{3+}, Li^+ that may be used to eliminate the flickering luminosity of AC LEDs [9]. Yihua Hu et al. reported about self-reduction of Ce^{4+} when calcined in the open atmosphere during the process of preparation of $Y_{2.95}Al_5O_{12}$:Ce^{4+}0.05, Which makes $Y_{2.95}Al_5O_{12}$:Ce^{4+}0.05 phosphor emit yellow color (~531 nm) under excitation of blue light, for the reason that a part of Ce^{4+} has been reduced into Ce^{3+} [10,11]. The solution combustion method has been used to synthesize Ce^{3+} doped $SrAl_2O_4$, and its photoluminescence characteristics have been reported [12]. Significantly, the interaction between electrons and phonons contributes to the explanation of the temperature-dependent increase in the dielectric constant. The higher dielectric constant value is due to stronger space charge polarisation in lower frequency regions. This might be described using a polarisation mechanism similar to the conduction process. The polarisation is produced by the local displacement of the applied field caused by the electrical exchange of the number of ions in the materials. The point at which the space charge can no longer support and conform to the external field is as frequency rises. A low dielectric constant is frequently preferred for a variety of applications, such as high-speed integrated packages, which call for materials with a dielectric constant of less than 3.5 and minimal dielectric loss, and satellite communication applications, which need materials with a dielectric constant of 2.5 [13–18].

In this paper, $SrAl_2O_4$ is used as the host material and is doped with different concentrations of stimulator Ce^{3+} to make phosphors through the solid-state reaction method under different annealing temperatures. The luminescence properties and their basic characteristics such as the structural, optical, and morphology of the synthesized materials are examined in detail.

2. Experimental

$Sr_{(1-x)}$ Al_2O_4:xCe^{3+} phosphors were prepared by considering the good quality chemicals using the solid-state reaction (SSR) method. The molecular weight percentage of the elementary materials such as strontium carbonate ($SrCO_3$; Sigma Aldrich), aluminum oxide (Al_2O_3; Alfa Aesar), and Cerium oxide (CeO_2; sigma) were mixed in cognate for an hour. With the addition of a small quantity of ethanol to the synthesized mixture, the entire composition was moved to alumina crucibles (area = 18.23 cm^2) and was kept in a furnace for 12 h with the temperature set at 1100 C (Ramping rate of the furnace: 5 °C/min) under ambient conditions. The obtained powders were reground and heated at 1200 °C for 12 h in a reducing atmosphere where carbon powder (reduction agent) was kept around the alumina crucible. This sample was crushed further for 15 min was subjected to different characterizations.

3. Characterization techniques

The crystalline phase of the prepared material was identified by X-ray diffraction (XRD; PANalytical) with Cu-Kα1 radiation of

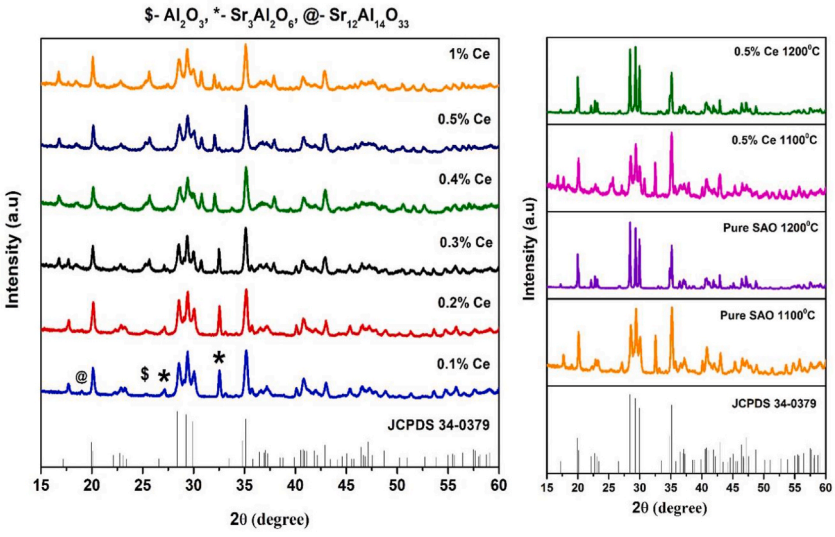

Fig. 1. XRD structural pattern, (left) SAO: x Ce ((x = 0.1, 0.2, 0.3, 0.4, 0.5, 1% MW %) powder, (right) pure SAO and 0.5% Ce doped SAO phosphors at two different temperature.

wavelength (λ = 1.5406 Å), under a preset voltage and current values of 40 kV and 40 mA respectively. The surface morphology of this sample was recorded in field emission scanning electron microscopy (FESEM, Hitachi 6600). Micro Raman spectrometer (HORIBA) was used for the Raman spectroscopic analysis with Nd:YAG semiconductor laser excitation of 532 nm. The vibrational spectroscopic analysis was further conducted using Fourier transformed infrared (FTIR) spectroscopy (Bruker, Alpha T), and their composition profile was examined using X-ray Photoelectron Spectroscopy (XPS) (ULVAC-PHI, PHI 5000 version probe III). X-ray photoelectron spectroscopy was performed at a base pressure of 1× 10-7 Pa equipped with the AlKα emission line (1486.6 eV). Using a 450 W xenon lamp excitation source, photoluminescence (PL) spectra of the sample were recorded in a spectrofluorometer (Horiba- Fluorolog BFL3-111). Electrical studies were examined by using HIOKI- LCR METER IM 3536 instrument in the frequency range from 4 Hz to 8 MHz at different temperatures.

4. Result and discussion

The X-ray diffraction (XRD) pattern in Fig. 1, shows the presence of a monoclinic $SrAl_2O_4$ phase with P_{21}, which matches with JCPDS file No. 34–0379 [19]. The addition of Ce^{3+} (ionic radius 0.101 nm) ions in the crystal lattice, with a similar radius of Sr^{2+} (ionic radius) 0.126 nm)' has not modified the crystal structure [20] which was evident from the peak of the XRD spectra [21]. The crystal structural phase of the final product is found by the planes (011), (−211), (220), (211), and (031) attributed to major peaks at 2θ values of 19.96°, 28.39°, 29.29°, 29.93° and 35.14°, respectively. In addition to this, the peaks between 28 and 30° correspond to the minor secondary structural phase formation of $Sr_4Al_{14}O_{25}$ and $Sr_3Al_2O_6$ [22,23].

The moderate grain size (D) of the particles is calculated from the broadening peaks observed in the crystal lattice as in equation (1) quoted by Scherrer [24].

$$D = 0.9\lambda/\beta \cos\theta \tag{1}$$

The crystallite size of the prestine $SrAl_2O_4$ and 0.1, 0.2, 0.3, 0.4, 0.5, and 1 MW% Ce^{3+} doped $SrAl_2O_4$ is calculated to be ~51 nm, ~55 nm, ~52 nm, ~54 nm, ~56 nm, ~57 nm, and ~53 nm, respectively. The lattice parameter (a = 8.44 Å, b = 8.82 Å, c = 5.145 Å) are calculated using equation (2), which is confirmed by Rietveld refinement with the goodness of fit $\chi^2 = 5.1$, as shown in Fig. 2. Obtained parameters by Rietveld refinement are recorded in Table 1.

$$\frac{1}{d^2} = \frac{1}{sin^2\,\beta}\left\{\frac{h^2}{a^2} + \frac{k^2\,sin^2\,\beta}{b^2} + \frac{l^2}{c^2} - \frac{2hl\cos\beta}{ac}\right\} \tag{2}$$

Raman spectroscopy analysis is used to find numerous modes of vibrations present in the sample. The Raman spectrum of the 0.5% Ce doped $SrAl_2O_4$ sample is displayed in Fig. 3. The characteristic peak is around 465 cm^{-1}, attributed to the bending mode of O–Al–O bonds in corners distribution along $[AlO_4]^{5-}$ tetrahedral, which is representing the polymorphs existing in the synthesized sample [25]. A significant fact is that the peak value is obtained at 465 cm^{-1} in the non-crystallized arrangement, when the sample was annealed at low temperatures, which recommends that the $[AlO_4]$ unit is stabilized first as a rigid unit, whereas the derangement occurs only from the orientation of such units with minor oxygen shifts. The minor peak around 175 cm^{-1} represents tetrahedral tilts [26].

Fig. 4 (a, b) displays the FESEM image pure and 0.5 MW% Ce doped $SrAl_2O_4$ phosphors at 200 nm magnification. In pure $SrAl_2O_4$ sample exhibits an irregular structure with lots of holes and spaces which arises due to the emission of gases during the synthesis process [27]. The morphology of the sample is changed from a needle-like structure to a shiny plate structure while doped with Ce, as displayed in Fig. 4 (b), this means that Ce^{3+} ions favor plate-like structure and also have smaller ionic radii than that of Sr^{2+} ion. This is

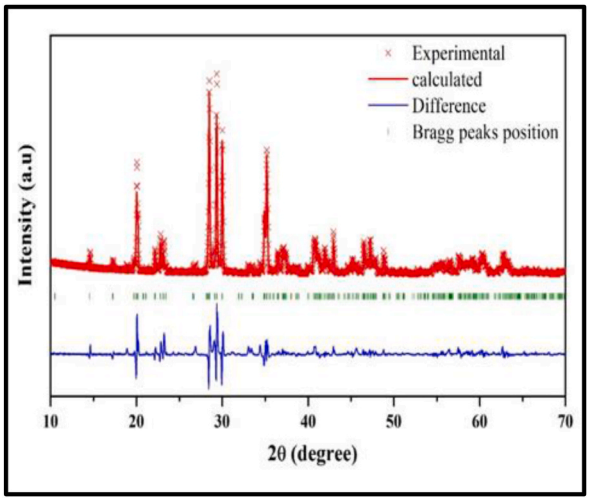

Fig. 2. Rietveld refinement pattern.

Table 1
Structural parameter.

Compound	$SrAl_2O_4$
Structural Parameters	
a, b, c (Å)	8.42,8.81, 5.14
α, β, γ (°)	90, 93.38, 90
Space group	P_{21}
Structure	Monoclinic
Goodness of fit (χ^2)	5.1

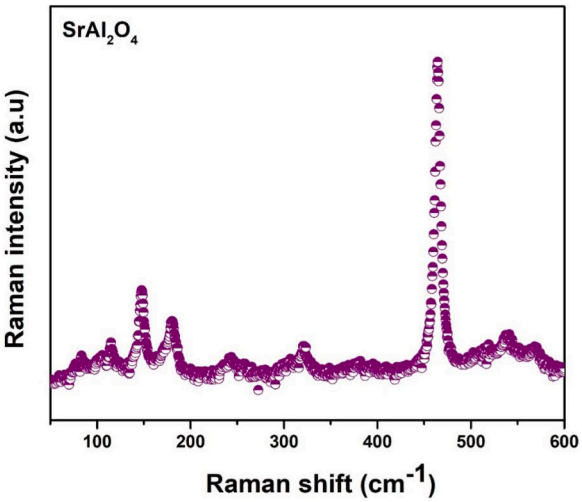

Fig. 3. Raman spectrum of 0.5 MW% Ce doped $SrAl_2O_4$.

associated with the change in morphology to plates [2]. The plate-like structure shows luminescent properties when compared with other irregular structures [28,29].

Fig. 5 displays the FTIR spectrum of the $SrAl_2O_4$ phosphors obtained for a 0.5 MW% Ce. A firm absorption band around at 3455 and 3424 cm^{-1} rising from O–H stretching and the bending mode vibration of water due to atmospheric conditions. The bands between 500 cm^{-1} and 1000 cm^{-1} corresponds to the IR active vibration modes of SAO. The symmetric and antisymmetric stretching bands of phosphors appeared between 418 cm^{-1} and 483 cm^{-1} with the peaks at 536 cm^{-1}, 711 $cm^{-,1}$ and 646 cm^{-1} representing the O–Al–O and Sr–O vibrations, respectively. The two bands at 1478 cm^{-1} and 1639 cm^{-1} are appropriate to the C–O vibrations [30]. The FTIR stretching and vibration results confirm the existence of Sr, Al, and O components in $SrAl_2O_4$ phosphors.

XPS analysis of 0.5 MW% Ce doped $SrAl_2O_4$ phosphor is shown in Fig. 6. The chemical elements (like C 1s, O 1s, Sr 3d, Al 2p, and Ce 3d) of phosphor are found in the photoelectron signals. The reference signal C 1s is observed around 285.1 eV and 289.7 eV representing the existence of adventitious carbon due to atmospheric exposure of the sample. The binding energy value at 531.5 eV is represented as O 1s as a result of the formation of metal oxides [31]. Binding energy at 74.1 eV is represented as Al 2p state present in the phosphor and two peaks present at 133.6 eV and 135.3 eV confirm the attendance of Sr 3d, which is in good agreement with the reported information [32]. Ce 3d spectrum has bi-peaks at higher binding energies. The peaks at 888.9 eV and 901.4 eV are corresponding to Ce $3d_{5/2}$ and Ce $3d_{3/2}$, respectively, which confirms the standard separation of Ce 3d valence state [33].

Fig. 7 displays the excitation spectrum of 0.5 MW% Ce doped $SrAl_2O_4$ phosphor recorded in the range between 250 nm and 450 nm. The excitation spectrum at 256 nm is ascribed to the transition of 4f-5d from the ground state of Ce^{3+} ion which corresponds to the transition from the $^2F_{5/2}$ ground state to the different excited states such as $^2D_{3/2}$ and $^2D_{5/2}$ respectively.

The photoluminescence emission spectra of as-synthesized phosphors were observed between 300 nm and 900 nm. Fig. 8 shows the emission spectra of 0.1 MW% and 0.5 MW% Ce^{3+} doped $SrAl_2O_4$ phosphors, recorded using an excited wavelength of 256 nm. The sample reveals three major peaks at ~420 nm, ~490 nm, and ~610 nm which are significant transitions of 4f-5d transitions of $^2D_{5/2}$ and $^2D_{3/2}$ to $^2F_{5/2}$ transitions, respectively [2]. The combination of transition is well known resulting in near white light emission of Ce^{3+} element due to the magnetic dipole transition which is intensely influenced by the ligand field around the Ce^{3+} dopant ion site [34]. Since the emission intensity of the $^2D_{5/2} \rightarrow {}^2F_{5/2}$ (blue region) is more intense compared to $^2D_{3/2} \rightarrow {}^2F_{5/2}$ (green region) peak on account of Ce^{3+} ions located at the high symmetry site in the host with an inversion center however, the blue region exhibits higher intensity when Ce^{3+} ions detected at a low symmetry site (without an inversion center).

The critical energy distance (R_c) can be found using Blasse Eq. (3) [35].

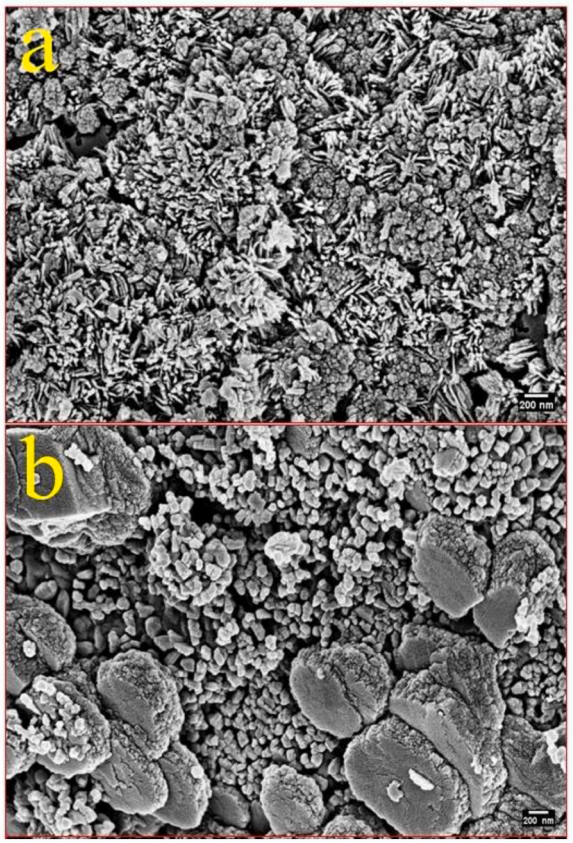

Fig. 4. FESEM image for pure SAO, SAO: 0.5 MW% Ce phosphors.

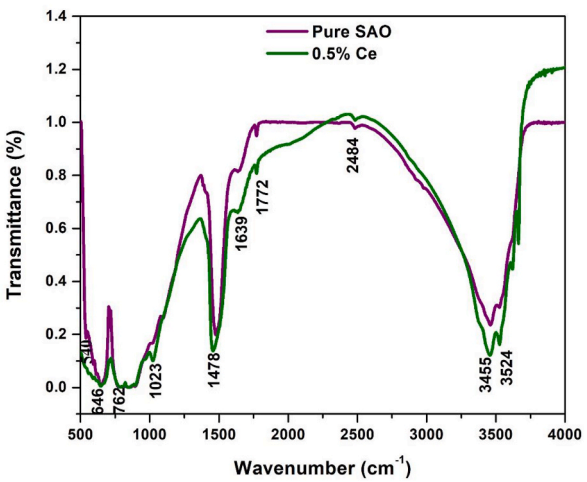

Fig. 5. FTIR spectra of pure $SrAl_2O_4$, 0.5 MW% Ce^{3+} doped $SrAl_2O_4$.

$$R_C = 2 \times \sqrt[3]{\left[\frac{3V}{4\pi N X_c}\right]} \tag{3}$$

here N represents the number of Z cations in the unit cell (i.e. 4), V is the Volume of the unit cell = 383.8×10^{-3} nm and X_c is the critical concentration = 0.5.

Non-radiative energy transfer between the doping ions can point to either electric multipolar/exchange interactions due to the

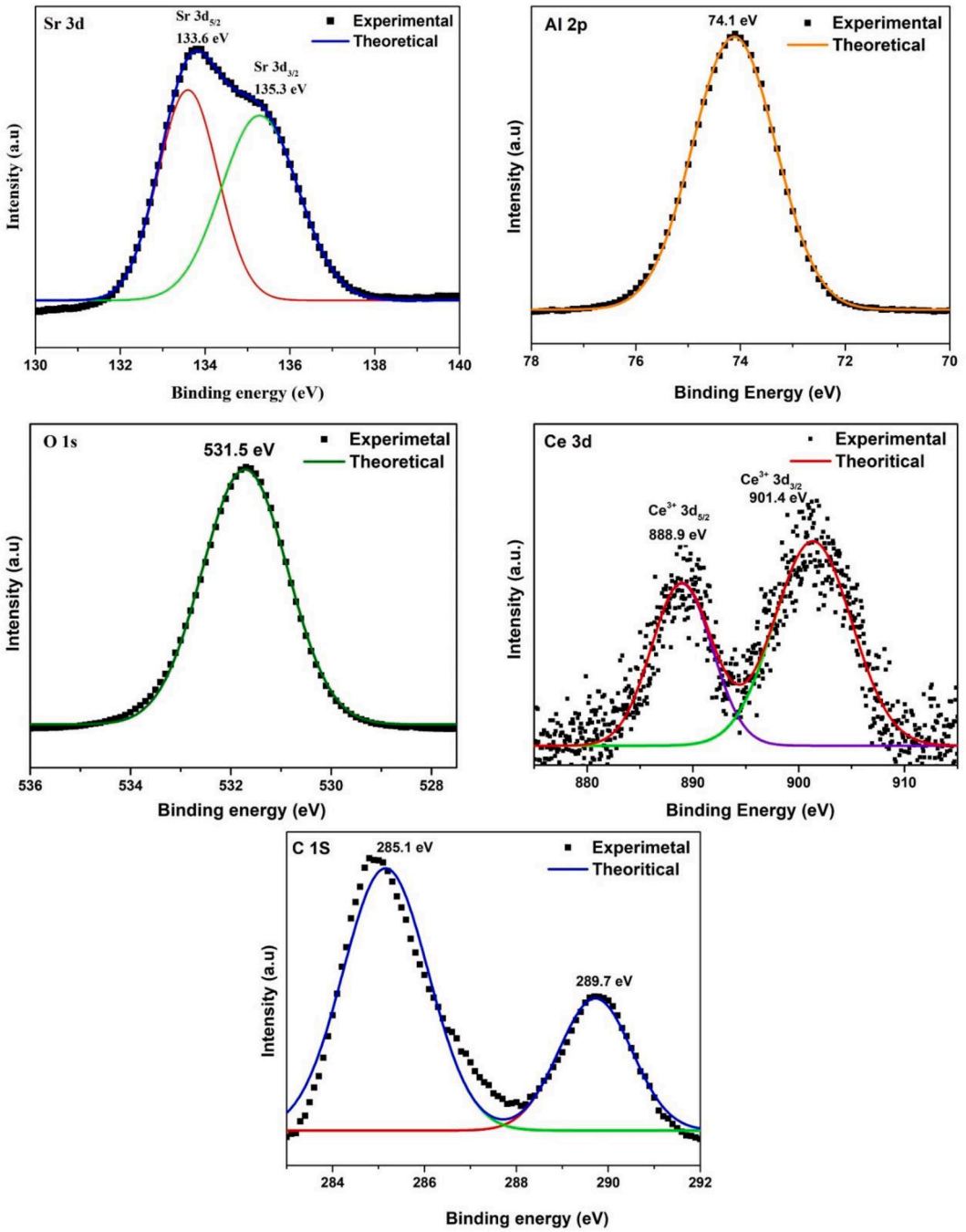

Fig. 6. XPS spectra for 0.5 MW% Ce doped SAO phosphor.

interaction between Ce^{3+} ions being stimulated by increasing doping concentration. Either exchange interactions occur at a smaller value of R_c (<0.5 nm), or electric multipolar interactions prevail. In the case of $SrAl_2O_4$: Ce^{3+} phosphors, the value of R_c was calculated to be 1.540 nm, hence the sample exhibits electric multipolar interactions [36].

Fig. 9 displays the Commission Internationale de L'Eclairage (CIE) chromaticity graph of the $SrAl_2O_4$:xCe^{3+} sample, for analyzing the precise emission colour and its purity of the as-synthesized $SrAl_2O_4$:xCe^{3+} phosphors. The CIE chromaticity coordinates (x = 0.23002, y = 0.21383) of the phosphors are specified in Fig. 9, which are symbolized by a cross mark. The emission colour is found in the white region for the $SrAl_2O_4$: xCe^{3+} phosphors displayed in Fig. 8. Since these outcomes, it is confirmed that the as-synthesized $SrAl_2O_4$:xCe^{3+} phosphors are apt for white light emission under near ultraviolet excitation wavelength [34,37].

The colour quality of the synthesized phosphor is found by correlated colour temperature (CCT) calculations, which describe the

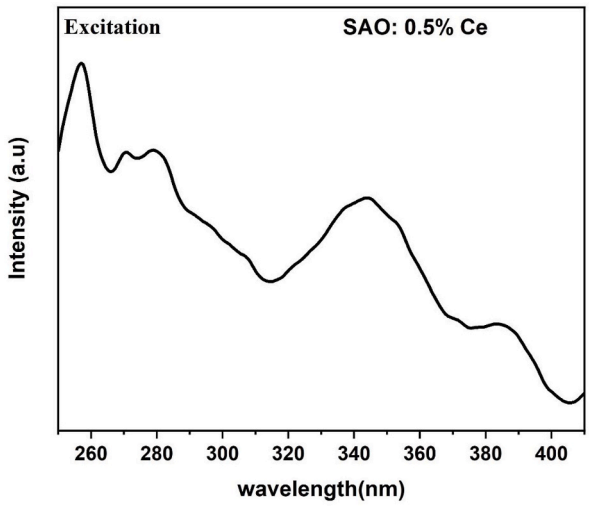

Fig. 7. Photoluminescence excitation spectrum for 0.5 MW% Ce doped $SrAl_2O_4$ phosphor.

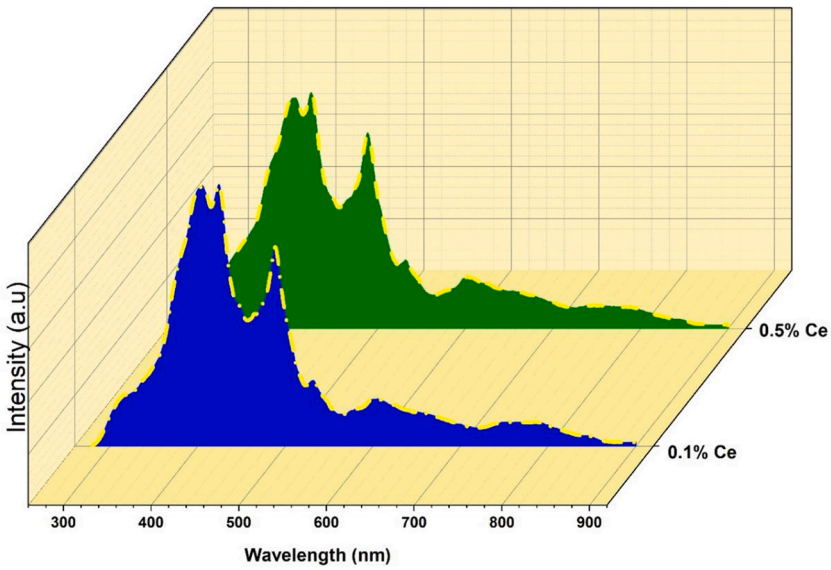

Fig. 8. Photoluminescence emission spectrum of synthesized phosphors.

colour produced by a light source and is calculated from McCamy empirical Eq. (4) [38].

$$CCT = -449n^3 + 3525n^2 - 6823.3n + 5520.33 \quad (4)$$

where, $n = \frac{x-x_e}{y-y_e}$, $x_e = 0.332$, $y_e = 0.186$, is the epicenter

A source with a CCT value below 3000 K is typically treated as a "warm" lamp, whereas those with a CCT value greater than 4000 K are considered as "cool'' sources [39]. The calculated CCT value of the present synthesized 0.5 Ce^{3+} doped SrAl2O4 phosphor is 1503 K, which is in warm appearance. The outcomes show the potential of the as-synthesized phosphors for a display device and white light emitting diodes (WLEDs) applications.

The investigation of the dielectric properties of material plays a major role in the field of super capacitors, energy storage, opto-electronics, LEDs, ferroelectrics, etc., [40,41]. The dielectric constant and loss tangent for the $SrAl_2O_4$:0.5% Ce^{3+} phosphor was investigated as a function of frequency in the range of 4 Hz–8 MHz with different temperatures as shown in Figs. 10 and 11. The values of the dielectric constant appear initially random for the current sample in the low frequency range a large frequency dispersion in dielectric constant was discovered, which might be attributed to cation valency fluctuations and space charge polarisation at the sample electrode interface and grain, but it shows stable values from 3 kHz to 8 MHz. According to Koop's hypothesis, the applied frequencies inflict a major impact in dielectric properties [42]. Generally, the dispersion in dielectric constant may also be caused by

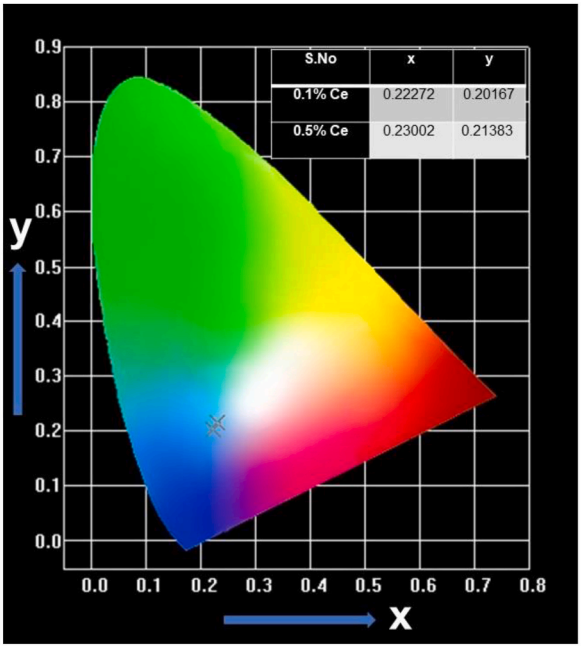

Fig. 9. CIE coordinates of synthesized phosphor.

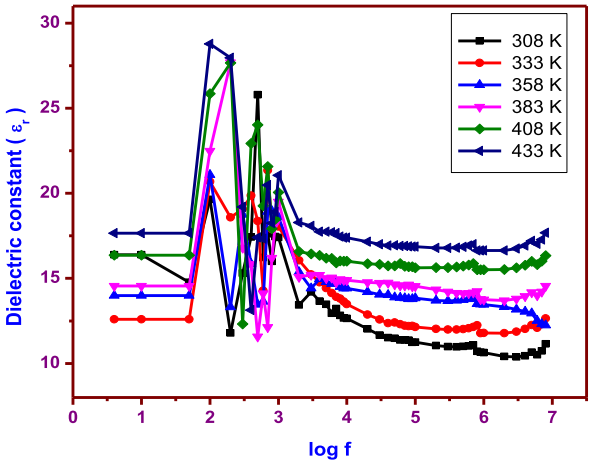

Fig. 10. Showing dielectric constant variations at different temperatures with various frequencies for $SrAl_2O_4$:0.5% Ce^{3+} phosphor.

the hopping exchange of charges between two localised states which is controlled by its density and the subsequent displacement of charges with the applied field. The fact that electron exchange between two metal ions cannot follow the variation of external ac field at higher frequency and thus attributed to the stability of the dielectric constant and loss tangent at the higher end of frequency [43] whereas, the dipolar and interfacial polarisation determine the lower frequency. At higher frequency, dielectric constants are dictated by electronic and ionic polarisation but dipoles owing to interfacial polarisation or space charge polarisation cannot retort [44,45]. For the conduction process, grain boundaries have a stronger influence than at low frequencies. The dielectric constant is higher at thin grain boundaries and this value at low frequency might be attributed to the inhomogeneous structure of dielectric induced by grain boundaries and porosity [46]. Similarly, the loss tangent exhibits frequency-dependent dispersion. The existence of space charge at the sample electrode interface and grain boundaries was confirmed by the presence of substantial dielectric loss at low frequency. The non-uniform accumulation at the grain boundaries and sample electrode contact may be due to space charge polarisation. It is known that the loss tangent is connected to mechanisms of resistive loss and relaxation loss. This leads in nearly same values of dielectric constant and loss tangent behaviour at higher frequencies.

Figs. 12 and 13 show the fluctuation of dielectric constant and loss tangent with temperature for the present samples at 10^2 Hz, 10^3 Hz, 10^4 Hz, 10^5 Hz, and 10^6 Hz at temperatures ranging from 308 K to 433 K. The dielectric constant rises with increasing temperature

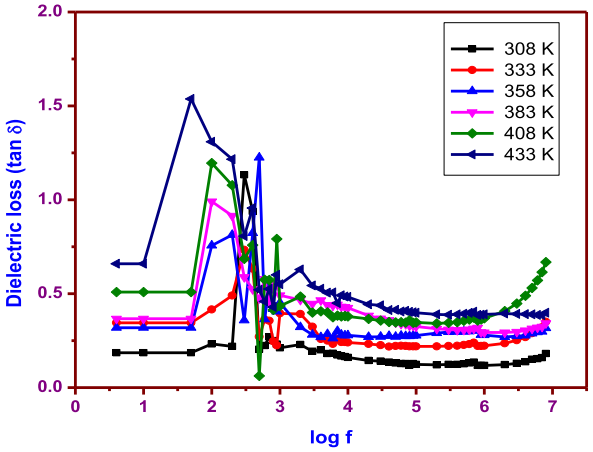

Fig. 11. Showing dielectric loss variations at different temperatures with various frequencies for $SrAl_2O_4$:0.5% Ce^{3+} phosphor.

because of thermally activated charges indicating the presence of hopping conduction in the materials, according to the examination of the dielectric dispersion curve. The electron-phonon interaction helps explain the rising trend of dielectric constant with temperature. At high temperatures, electric dipoles accumulate enough thermal energy to follow changes in the applied field, whereas at low temperatures, electric dipoles contribute minimally to polarisation. The observed trend of the present material shows minor variance. An electric dipole is formed, which increases the dielectric constant due to the creation of vacancies by the rare earth cations [47].

The studies of the loss tangent with temperature reveals that the loss tangent increases with increasing temperature for the present materials and is almost dependent on temperature. The dispersion behaviour of the loss tangent curve is similar to the dielectric constant because of the existence of thermally activated free charge carriers which might also be due to the existence of flaws such as aluminium vacancies and oxygen vacancies. Another important feature is conductivity, which dominates at higher temperatures, leading in increase in tan δ. In the case of Ce^{3+}, there is some deviation from the usual pattern of tan δ fluctuation with temperature.

The graph shows that conductivity increases with temperature at a wide range of frequencies. The increased σ_{ac} values with frequency due to the electrical activity of conductive granules at high frequencies and temperature might be explained by the changing polarisation behaviour of the dielectric materials (Fig. 14). When the thermal energy is on the order of the ion dipole interaction, the dissociation of ion charge and water molecules occurs, allowing for the escalation of thermally driven charge carriers. At elevated temperatures, electrical conductivity increased as a derivative of polarisation increasing owing to the simplicity that additional carriers of charge may collect in the lack of ion dipole connections [47]. The graph of ln σ_{ac} vs 1/T is shown in Fig. 15, and it follows the Arrhenius connection. As a consequence, based on the slope of the plot, the activation energy for ionic migration was determined and is shown in Fig. 16. The present materials utilised in high frequency applications are confirmed by the AC conductivity and loss tangent values.

5. Conclusion

The white light emitting $SrAl_2O_4$:xCe^{3+} phosphors are productively synthesized by the process of conventional solid-state reaction.

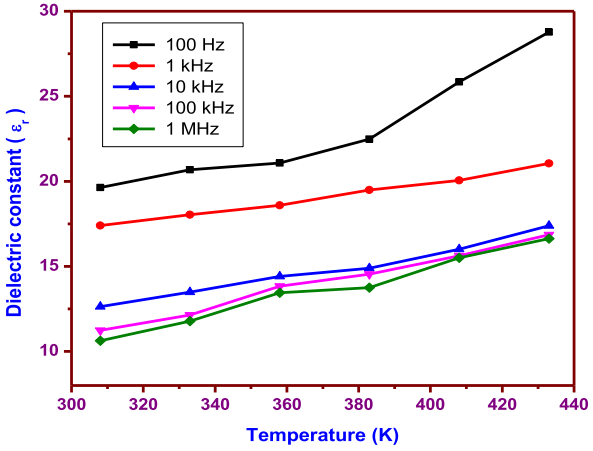

Fig. 12. Temperature dependence of dielectric constant for $SrAl_2O_4$:0.5% Ce^{3+} phosphor.

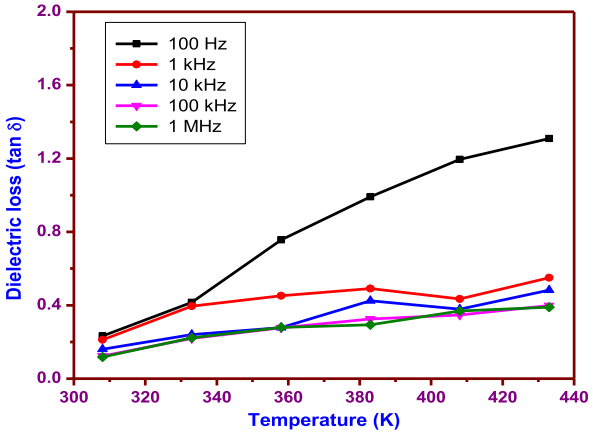

Fig. 13. Temperature dependence of dielectric loss for $SrAl_2O_4$:0.5% Ce^{3+} phosphor.

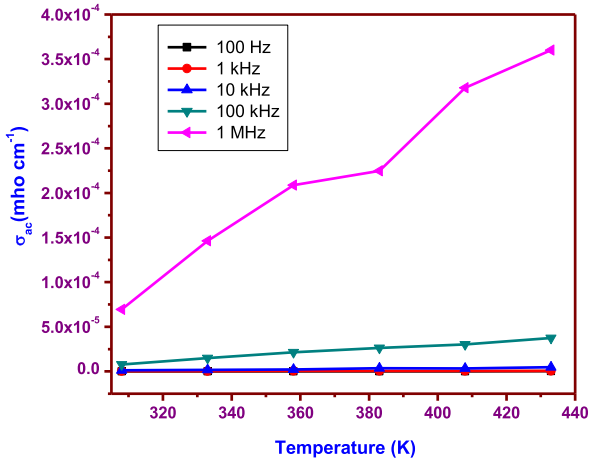

Fig. 14. Variation of ac-electrical conductivities with temperatures at different frequencies for $SrAl_2O_4$:0.5% Ce^{3+} phosphor.

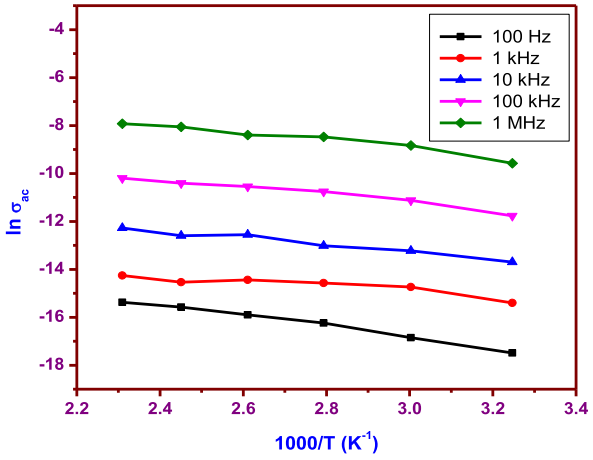

Fig. 15. Plot of ln (σ_{ac}) T versus 1000/T for $SrAl_2O_4$:0.5% Ce^{3+} phosphor.

The monoclinic phase of as-synthesized phosphors was verified by the XRD structural pattern and the phosphor thus emitted ~420 nm, ~490 nm, and ~610 nm under UV excitation of wavelength 256 nm due to the transition of $^2D_{5/2} \rightarrow {}^2F_{5/2}$, $^2D_{3/2} \rightarrow {}^2F_{5/2}$ and relaxed level to $^2F_{5/2}$, respectively. The white light emission was affirmed by CIE chromaticity x, y coordinates. CCT value is calculated and

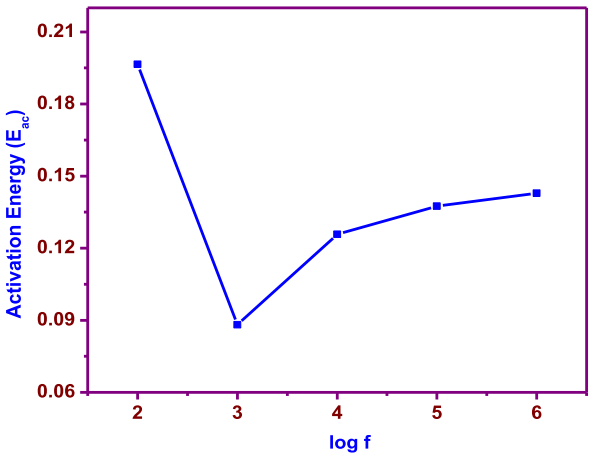

Fig. 16. Variation of ac activation energy with log frequency for $SrAl_2O_4$:0.5% Ce^{3+} phosphor.

observed in the acceptable limit and can be represented as the warm source. The $SrAl_2O_4$:0.5 MW% Ce^{3+} phosphor can be used as a white light source when compared to phosphors of 0.1 MW% and can be considered a probable applicant for white LEDs applications. The electron hopping is accountable for the dielectric polarisation in phosphor. The electron hopping plays an important role in deciding the function of dielectric constant and loss factor with frequency as well as temperatures and also activation energy was determined.

Author contribution statement

Ganesh Kumar. K: Conceived, designed the experiments; Performed the experiments; Wrote the paper.
Balaji Bhargav. P: Conceived and designed the experiments.
Sasikumar. P, Anitha Gopalan, Mary Anjalin. F: Contributed reagents, materials, analysis tools or data.
Pugazhendhi. S, Mohamed Abbas: Analyzed and interpreting the data.
Vimalan. M: Analyzed and interpreted the data; Wrote the paper.

Data availability statement

Data included in article/supplementary material/referenced in article.

Declaration of Competing interest

The authors declare that they have no known competing financial interests or personal relationships that could have appeared to influence the work reported in this paper.

Acknowledgements

This work was supported by SIMATS School of Engineering and SSN Trust- Sri Sivasubramaniya Nadar College of Engineering, Kalavakkam, Chennai, India by providing funding for the synthesis and characterization. The authors extend their appreciation to the Deanship of Scientific Research at King Khalid University (KKU) for funding this research through the Research Group Program Under the Grant Number:(R.G.P.2/513/44).

References

[1] M. Elsagh, M. Rajabi, E. Amini, Characterization of SrAl2O4:Eu^{2+}, Dy^{3+} phosphor nano-powders produced by microwave synthesis route, J. Mater. Sci. Mater. Electron. 25 (4) (2014) 1612–1619.
[2] L.A. Diaz-Torres, J. Oliva, D. Chavez, C.R. Garcia, Enhancing the white light emission of $SrAl_2O_4$: Ce^{3+} phosphors by co doping with Li^+ ions, Ceram. Int. 42 (14) (2016) 16235–16241.
[3] T.-P. Tang, C.-M. Lee, F.-C. Yen, The photoluminescence of $SrAl_2O_4$: Sm phosphors, Ceram. Int. 32 (6) (2006) 665–671.
[4] M. Avdeev, S. Yakovlev, A.A. Yaremchenko, V.V. Kharton, Transitions between P_{21}, and P6322 modifications of $SrAl_2O_4$ by in situ high-temperature X-ray and neutron diffraction, J. Solid State Chem. 180 (12) (2007) 3535–3544.
[5] M. Misevicius, J.E. Jorgensen, A. Kareiva, Sol-Gel synthesis, structural and optical properties of cerium-doped strontium aluminates, $Sr_3Al_2O_6$ and $SrAl_{12}O_{19}$, Mater. Sci. 19 (4) (2013) 1392–1398.
[6] R.E. Rojas-Hernandez, F. Rubio-Marcos, A. Serrano, A. Del Campo, J.F. Fernandez, Precise tuning of the nanostructured surface leading to the luminescence enhancement in SrAl2O4 based core/shell structure, Sci. Rep. 7 (1) (2017) 462.
[7] S. Singh, R.K. Kuraria, S.R. Kuraria, Photoluminescence Studies of Cerium Doped Strontium Aluminate Nanophosphors (SrAl2O4: Ce), vol. 2104, 2019, 020014.

[8] G. Li, Y. Lai, T. Cui, H. Yu, D. Liu, S. Gan, Luminescence properties and charge compensation of Sr3Al2O6 doped with Ce3+ and alkali metal ions, Mater. Chem. Phys. 124 (2–3) (2010) 1094–1099.
[9] Lei Chen, Yao Zhang, Fayong Liu, Anqi Luo, Zhixin Chen, Yang Jiang, Shifu Chen, Ru-Shi Liu, Mater. Res. Bull. 47 (2012) 4071.
[10] Mu Zhong-Fei, Yin-Hai Wang, Yi-Hua Hu, et al., The afterglow and thermoluminescence properties of $Y_3Al_5O_{12}$: Ce^{3+}, Acta Phys. Sin. 60 (1) (2011), 013201.
[11] Zhongfei Mu, Yihua Hu, Li Chen, Xiaojuan Wang, Enhanced red emission in Sr_2CeO_4: Eu^{3+} by charge compensation, J. Electrochem. Soc. 158 (10) (2011) J287–J290.
[12] K.E. Foka, F.B. Dejene, H.C. Swart, Phys. B Condens. Matter 439 (2014) 177.
[13] S. Tamilselvan, M. Vimalan, I. Vetha Potheher, R. Jeyasekaran, F. Yogam, J. Madhavan, Generation of 532 nm laser radiation and Phase matching properties of organic nonlinear optical material, Optik 125 (2014) 164–169.
[14] Ginson P. Joseph, K. Rajarajan, M. Vimalan, S. Selvakumar, S.M. Ravi Kumar, J. Madhavan, P. Sagayaraj, Spectroscopic, thermal and mechanical behavior of allylthiourea cadmium chloride single crystals, Mater. Res. Bull. 42 (2007) 2040–2047.
[15] T. Sujatha, A. Cyrac Peter, M. Vimalan, J. Merline Shyla, J. Madhavan, Thermal, mechanical, optical and conductivity studies of a novel NLO active L-phenylalanine L-phenylalaninium dihydrogenphosphate single crystal, Phys. B Condens. Matter 405 (2010) 3365–3370.
[16] J. Maalmarugan, R. Zema Ferin, G. Joesna, A. Mustafa, M. Gulam Mohamed, M. Bououdina, D. Sankar, M. Vimalan, K. SenthilKannan, In situ grown ZnO nanoparticles using Begonia leaves–dielectric, magnetic, filter utility and tribological properties for mechano-electronic applications, Appl. Phys. A 128 (2022) 217.
[17] P. Saravanan, K. SenthilKannan, A. Mustafa, M. Vimalan, M. Bououdina, Dielectric and magnetic properties of Allium cepa and Raphanus sativus extracts biogenic ZnO nanoparticles, J. Mater. Sci. Mater. Electron. 32 (2021) 590.
[18] Amrut S. Lanje, Satish J. Sharma, Raghumani S. Ningthoujam, J.-S. Ahn, Ramchandra B. Pode, Low temperature dielectric studies of zinc oxide (ZnO) nanoparticles prepared by precipitation method, Adv. Powder Technol. 24 (2013) 331–335.
[19] K. Ganesh Kumar, P. Balaji Bhargav, K. Aravinth, R. Arumugam, P. Ramasamy, Dysprosium activated strontium aluminate phosphor: a potential candidate for WLED applications, J. Lumin. (2020), 117126.
[20] G. Swati, S. Chawla, S. Mishra, B. Rajesh, N. Vijayan, B. Sivaiah, A. Dhar, D. Haranath, Investigation on luminescence enhancement and decay characteristics of long afterglow nanophosphors for dark-vision display applications, Appl. Surf. Sci. 333 (2015) 178–185.
[21] I.P. Sahu, D.P. Bisen, N. Brahme, R.K. Tamrakar, Generation of white light from dysprosium-doped strontium aluminate phosphor by a solid-state reaction method, J. Electron. Mater. 45 (4) (2016) 2222–2232.
[22] Byung-Geon Park, Characteristics of Eu^{2+}, Dy^{3+} Doped $SrAl_2O_4$ synthesized by hydrothermal reaction and its photocatalytic properties, J. Mater. Sci. Chem. Eng. 6 (2018) 12–21.
[23] Yuting Yang, Hongyi Jiang, Xu Dong, Hai Ou, Ting Yang, Preparation of SrAl2O4:Eu^{2+}, Dy^{3+} phosphors using propylene oxide as gel agent and its optical properties, Mater. Res. Express 5 (2018), 016201.
[24] B.D. Cullity, Elements of X-Ray Diffraction, second ed., Addison-Wesley Publishing Company, Inc. Philippines, 1978.
[25] P. Escribano, M. Marchal, M.L. Sanjuan, P. Alonso-Gutierrez, B. Julian, E. Cordoncillo, Low-temperature synthesis of $SrAl_2O_4$ by a modified sol-gel route: XRD and Raman characterization, J. Solid State Chem. 178 (6) (2005) 1978–1987.
[26] M. Ayvacikli, A. Ege, S. Yerci, Can, N, Synthesis and optical properties of Er^{3+} and Eu^{3+} doped $SrAl_2O_4$ phosphor ceramic, J. Lumin. 131 (2011) 2432–2439.
[27] Reza Zamiri, A.F. Lemos, Avito Reblo, , Hossein Abbastabar Ahangar, J.M.F. Ferreira, Effects of rare-earth (Er, La and Yb) doping on morphology and structure properties of ZnO nanostructures prepared by wet chemical method, Ceram. Int. 40 (1) (2014) 523–529.
[28] Y.-F. Xu, D.-K. Ma, M.-L. Guan, X.-A. Chen, Q.-Q. Pan, S.-M. Huang, Controlled synthesis of single-crystal $SrAl_2O_4$:Eu^{2+}, Dy^{3+} nanosheets with long-lasting phosphorescence, J. Alloys Compd. 502 (1) (2010) 38–42.
[29] Arun Kumar, Garima Kedawat, Pawan Kumar, Jaya Dwivedi, Bipin Kumar Gupta, Sunlight-activated Eu^{2+}/Dy^{3+} doped $SrAl_2O_4$ water resistant phosphorescent layer for optical display and defense applications, New J. Chem. 39 (2015) 3380–3387.
[30] K.E. Foka, F.B. Dejene, H.C. Swart, Photoluminescence properties of Ce^{3+}-doped $SrAl_2O_4$ prepared using the solution combustion method, Phys. B Condens. Matter 439 (2014) 177–180.
[31] Xiaowen Zhan, Lai Shen, Steven G Greenbaum Mallory P Gobet, Mona Shirpou, Defect chemistry and electrical properties of garnet-type $Li_7La_3Zr_2O_{12}$, Chem. Phys. 20 (2018) 1447–1459.
[32] Xiaoming Liu, Xueya Chen, Yizu Li, Bingquan Wu, Xubiao Luo, Sheng Ouyang, Shenglian Luo, Kheraif Al, A. Abdulaziz, Lin, A g-C 3N 4@ Au@SrAl2O4:Eu2+, Dy3+ composite as an efficient plasmonic photocatalyst for round-the-clock environmental purification and hydrogen evolution, J. Mater. Chem. 7 (32) (2019) 19173–19186.
[33] F. Chen, X. Wang, Y. Nie, Q. Li, J. Ouyang, Z. Feng, V.G. Harris, Ferromagnetic resonance induced large microwave magnetodielectric effect in cerium doped $Y_3Fe_5O_{12}$ ferrites, Sci. Rep. 6 (1) (2016).
[34] M. Naseem Siddique, A. Ahmed, S.K. Riyajuddin, M. Faizan, K. Ghosh, P. Tripathi, Exploring the Ce3+ ions doping effect on optical and magnetic properties of NiO nanostructures, J. Magn. Magn Mater. (2019), 166323.
[35] Arumugam Raja, R. Nagaraj, K. Ramachandran, V. Sivasubramani, G. Annadurai, D. Joseph Daniel, P. Ramasamy, A novel bifunctional Dy^{3+} activated $RbCaF_3$ single phase phosphor: facile synthesis and dual-luminescence properties for WLEDs and dosimetry applications, Adv. Powder Technol. 31 (7) (2020) 2597–2604.
[36] Gattupalli Manikya Rao, G. Seeta Rama Raju, Sk Khaja Hussain, E. Pavitra, P.S.V. Subba Rao, Jae Su Yu, Tunable emissions via white-region from $Sr_2Gd_8(SiO_4)_6O_2$: RE^{3+} (RE^{3+}: Dy^{3+}, Tm^{3+}, Eu^{3+}) phosphors, New J. Chem. 40 (2016) 6214–6227.
[37] T. Matsuzawa, Y. Aoki, N. Takeuchi, Y. Murayama, A new long phosphorescent phosphor with high brightness, SrAl2O4:Eu2+, Dy3+, J. Electrochem. Soc. 143 (8) (1996) 2670–2673.
[38] Zhi-Wei Zhang, Xin-Yuan Sun, Lu Liu, You-shun Peng, Xi-hai Shen, Wei-Guo Zhang, Dong-Jun Wang, Synthesis and luminescence properties of novel $LiSr_4(BO_3)_3$: Dy^{3+} phosphors, Ceram. Int. 39 (2013) 1723–1728.
[39] I.P. Sahu, D.P. Bisen, N. Brahme, R.K. Tamrakar, Generation of white light from dysprosium-doped strontium aluminate phosphor by a solid-state reaction method, J. Electron. Mater. 45 (4) (2016) 2222–2232.
[40] Thangaraj Venkatesan, Jih-Hsing Chang, Mohd Shkir, K. Mohanraj, K. Thirumalai, M. Swaminathan, S. Sumathi, N. Valarmathi, C. Rajendran, Araichimani Arun, Sol-gel synthesis, characterization, dielectric and anti-bacterial properties of soft ferromagnetic oxide system $Gd_{4-x}Sr_{1+x}Fe_{5-x}Zn_xO_{14+\delta}$ [$0 \leq x \leq 0.45$], Inorg. Chem. Commun. 125 (2021), 108432.
[41] K. Suganya, J. Maalmarugan, R. Manikandan, T. Sakthi Nagaraj, R.P. Patel, K. Tamilarasi, M. Vimalan, K. SenthilKannan, Synthesis, studies of 2-benzyl-amino-4-p-tolyl-6,7-dihydro 5H-cyclo-penta–[b]pyridine-3 carbo-nitrile (BAPTDHCPCN) crystals for optical, photonic and mechano-electronic uses, J. Mater. Sci. Mater. Electron. 33 (2022) 19320–19330.
[42] G. Joesna, P. Saravanan, R. Zema Ferin, T. Gunachitra, D. Sankar, S. Tamilselvan, M. Meena, K. SenthilKannan, M. Vimalan, M. Gulam Mohamed, Domestic microwave supported green synthesis of ZnO nanoparticles for electronic, mechano, rheological and frequency intensifying applications, J. Mater. Sci. Mater. Electron. 33 (2022) 14144–14158.
[43] M.M. Rhaman, M.A. Matin, M.A. Hakim, M.F. Islam, Optical and electrical properties of impurity-less multiferroic bismuth ferrite nanoparticles, Mater. Sci. Eng. B 275 (2022), 115501.
[44] J. Maalmarugan, R. Zema Ferin, G. Joesna, A. Mustafa, M. Gulam Mohamed, M. Bououdina, D. Sankar, M. Vimalan, K. SenthilKannan, In situ grown ZnO nanoparticles using Begonia leaves–dielectric, magnetic, filter utility and tribological properties for mechano-electronic applications, Appl. Phys. A 128 (2022) 217.

[45] X. Vasanth Winston, D. Sankar, K. SenthilKannan, M. Vimalan, T. Rajesh Kumar, Gamma ray-irradiated induced effects on SCN ligandbased MMTC single crystals for optoelectronic applications synthesized by SR method, J. Mater. Sci. Mater. Electron. 33 (2022) 20616–20630.
[46] Shilpa Taneja, Preeti Thakur, Rakesh Kumar, S. Hemalatha, Yassine Slimani, Blaise Ravelo, Atul Thakur, Nanostructured rare earth Nd^{3+}doped nickel–zinc–bismuth spinel ferrites: structural, electrical and dielectric studies, Ceram. Int. 48 (19) (2022) 27731–27738.
[47] R. Divya, J. Maalmarugan, R.P. Patel, M. Meena, P.Nikolova Maria, M. Vimalan, S. Tamilselvan, K. SenthilKannan, Synthesis, experimental and computational characterizations of 8,9-dimethoxybenzo[b]naphtho[2,3-d] thiophene (DBNT) crystals for electro-mechano utilities, Inorg. Chem. Commun. 138 (2022), 109249.